JOURNAL OF COMPUTATIONAL PHYSICS 114, 339–349 (1994)

# An Assessment of Spectral Nonoscillatory Schemes

AMBADY SURESH

*Sverdrup Technology, Inc., NASA Lewis Research Center, Cleveland, Ohio 44135*

Received July 16, 1993; revised February 15, 1994

A new spectral nonoscillatory interpolation scheme is proposed that achieves spectral accuracy in smooth regions and is nonoscillatory on piecewise discontinuous data. The essential idea behind the scheme is to increase the order of an ENO scheme in proportion to the number of points, wherever possible. Numerical experiments with the new scheme on interpolation, 1D advection, inviscid Burgers' equation, and 1D gas dynamics confirm the high resolution features of the scheme. Comparisons with the results of earlier spectral nonoscillatory schemes show that the new scheme is competitive both in efficiency and accuracy. 

## INTRODUCTION

Spectral nonoscillatory schemes have recently been introduced in the literature as schemes which are nonoscillatory on discontinuous data and at the same time achieve spectral accuracy in smooth regions of the flow. Some of the early ideas can be found in Gottlieb, Lustman, and Orszag [1], where a postprocessing technique is introduced that consists of subtracting simple discontinuous functions from the computed solution and smoothing the difference. A nonoscillatory spectral scheme was first introduced in Cai, Gottlieb, and Shu [2], where spectral convergence was demonstrated for the 1D inviscid Burgers' equation. In a recent paper, Cai and Shu [3] generalize and improve these schemes further and present results for the full Euler equations in one and two dimensions.

The essential idea in these methods is to locate regions of the domain containing discontinuities and use a simple representation of the discontinuity in these regions. This solution is subtracted from the numerical solution and a weak conventional filter is applied to the difference. In early work, the size and location of the single discontinuity was estimated from the spectrum of the numerical solution and a simple sawtooth function was used to represent the discontinuity. This turns out to be impractical for several discontinuities, since two functions with discontinuities at different locations may have the same asymptotic spectrum for large wave numbers. In more recent work, local methods are used to locate an interval containing the discontinuity, and an essentially nonoscillatory (ENO) finite difference solution is used to represent the function in this interval. The ENO solution serves as an added basis function through which the Gibbs phenomenon is avoided. Thus, this scheme blends spectral methods with nonoscillatory finite difference methods, boosting the latter to spectral accuracy in smooth regions.

In this paper, we first assess the performance of the spectral nonoscillatory scheme of Cai and Shu [3] on the approximation of a periodic function with smooth structure and several discontinuities. Then, we present another approach towards obtaining spectral accuracy in smooth regions from an ENO interpolant. The basic idea in this new approach is to increase the order of the ENO scheme in proportion to the number of points, wherever possible. This method has the advantage that it does not use explicit discontinuity detection nor conventional filtering. We compare the performance of this new nonoscillatory spectral interpolation scheme with the scheme of Cai and Shu [3]. We observe spectral accuracy in the smooth regions with both schemes.

The rest of the paper is devoted to application of the new spectral interpolation scheme to 1D advection, inviscid Burgers' equation, and 1D gas dynamics. For advection, two different approaches are presented. In the first, a third-order Runge–Kutta scheme is used for time integration and spectral accuracy demonstrated by choosing a very small time step. In the second approach, a Cauchy–Kowalewski procedure is used to obtain a scheme that is spectrally accurate in space and time. The extension to 1D gas dynamics is discussed next where the test problem is the interaction of a moving shock wave with a density disturbance. Finally, we present our conclusions and comments.

## SPECTRAL ENO APPROXIMATION

Let $u(x)$ be a piecewise $C^\infty$ function on $[0, 2\pi]$ with several discontinuities, and let $x_i = 2\pi(i+N)/(2N+1)$, $i = -N, N$, be the grid points. The problem consists of con-



0021-9991/94 $6.00

structing an approximation $v(x)$ to $u(x)$ from the $2N+1$ values $u_i = u(x_i)$. The accuracy of the approximation can be measured in several ways. One of the simplest is to compute the error

$$e_{i+1/2} = |u(x_{i+1/2}) - v(x_{i+1/2})| \tag{1}$$

and study its dependence on $\Delta x = 2\pi/(2N+1)$. If $e_{i+1/2}$ decays faster than any power of $\Delta x$, then the approximation is said to be spectrally accurate. At points of discontinuity of $u(x)$ these point errors are not well defined and then it is customary to delete such points from consideration.

We briefly describe the spectral nonoscillatory approximation scheme of Cai and Shu [3] (hereafter referred to as the USE scheme) below. The first step here is to locate intervals which contain discontinuities. On very coarse meshes this can be quite difficult, but on fine meshes the divided differences can usually be used to detect a discontinuity. For example, in [3] the following procedure is used. Let

$$t_j = \max(|u_j - u_{j-1}|, |u_{j+1} - u_j|). \tag{2}$$

If $t_j > \max(3t_{j-2}, 3t_{j+2}, \alpha)$ then it is concluded that the interval $[x_{j-1}, x_{j+1}]$ contains a discontinuity. The parameter $\alpha$ has to be adjusted depending on the number of points used in resolving the discontinuity. After one pass at discontinuity detection, it is usually necessary to postprocess these intervals so that each interval contains a minimum number of points (6–8) and intervals are separated by a minimum number of points (6–8).

Once all such intervals have been identified, an $m$th-order ENO interpolation scheme is used in these intervals. These disjoint intervals are pieced together in a smooth way as follows. Let $[x_l^1, x_r^1]$ and $[x_l^2, x_r^2]$ be two such intervals with $x_l^1 < x_r^1 < x_l^2 < x_r^2$. The ENO interpolation immediately provides $m+1$ values ($m$ derivatives and a function value) at $x = x_r^1$ and at $x = x_l^2$. The unique $(2m+1)$-degree polynomial that takes on these values at $x = x_r^1$ and $x = x_l^2$ is used to connect these two intervals. Within the framework of ENO this is not such a difficult task. Specifically, the connecting polynomial is the polynomial that interpolates $m+1$ points belonging to the stencil of $x_r^1$ and the $m+1$ points belonging to the stencil of $x_l^2$. The first and last intervals containing discontinuities are also pieced together so as to satisfy periodicity. The composite function $\phi(x)$, containing $m$th-order ENO interpolation in regions containing a discontinuity and smooth connecting polynomials in between, plays the role of an added basis function.

This composite function $\phi(x)$ is then subtracted from $u(x)$ at the grid points to give

$$w_j = u(x_j) - \phi(x_j). \tag{3}$$

The residuals $w_j$ are zero within intervals containing discontinuities and nonzero outside of these intervals. The key idea is that the underlying function $w(x)$ is smooth enough so that a spectral method can be applied to it. The discrete Fourier coefficients of $w(x)$ are calculated as

$$\hat{w}_k = \frac{1}{(2N+1)} \sum_{j=-N}^{N} w_j e^{-ix_j k}. \tag{4}$$

A conventional weak filter is applied to $w_k$ and the result is added to the basis function $\phi(x)$ to obtain the uniform nonoscillatory approximation as

$$v(x) = \phi(x) + \sum_{k=-N}^{N} \sigma_k \hat{w}_k e^{ikx}. \tag{5}$$

Note that $v(x)$ is not an interpolant since $v(x_j) \neq w_j$, in general. The filter function is somewhat arbitrary. In most computations, an exponential filter is chosen so that

$$\sigma_k = e^{-\alpha(k/N)^{2l}}, \tag{6}$$

where $\alpha$ is a constant chosen so that $\sigma_N$ is machine zero and $2l$ is called the order of the exponential filter. Usually the order of the filtering is between 10 and 16 in most computations.

Both filtering and discontinuity detection are essential for achieving spectral accuracy in this scheme. For a discontinuous function, the approximation without any filtering yields only polynomial accuracy. For a smooth function, if a discontinuity is detected by error, the approximation without filtering is globally only as accurate as the ENO solution. In the next section, another approach to attaining spectral accuracy in smooth regions is proposed that uses neither conventional filtering nor explicit discontinuity detection.

## A NEW SPECTRAL ENO INTERPOLATION SCHEME

Spectral accuracy is achieved here by a completely different approach. Consider first the interpolation of a smooth periodic function by an ENO scheme of locally varying order $m(N)$, where $m(N)$ is an increasing function. For such a scheme, the order of accuracy of the scheme increases with the number of points, giving rise to global spectral accuracy. Obviously $m(N) \leqslant 2N$. Moreover, there does not seem to be any inconsistency within the ENO framework that would preclude a locally varying order $m(N)$.

However, difficulties arise when such a scheme is applied to the interpolation of a discontinuous function. The assumption that discontinuities are separated by $r+1$

points of smoothness, where $r$ is the order of the ENO scheme, breaks down. To illustrate these difficulties in a concrete manner, consider a function with two discontinuities, one between $[x_k, x_{k+1}]$ and another between $[x_{k+p}, x_{k+p+1}]$, and we attempt to interpolate using a locally variable order ENO scheme with $m(N) \gg p$. For any interval $[x_j, x_{j+1}]$ with $k+p > j > k$, due to stencil selection away from discontinuities, the leftmost point of the stencil $i(j)$ eventually becomes $i(j) = k+1$ and the rightmost point of the stencil becomes $k+p$. This corresponds to $m = p-1$. At the next step ($m = p$), the ENO scheme has to decide between $i(j) = k$ or $i(j) = k+1$, both of which involve stencils that interpolate across a discontinuity. If the stencil is allowed to grow unchecked, the scheme will pick one of these stencils, which will result in an oscillatory interpolant.

This difficulty can be overcome by a simple modification of the stencil selection procedure of the ENO scheme. At each step of the stencil selection process, we monitor the size of the two divided differences that are being compared. If both are large compared to some threshold ($1/\Delta x$, for example) then the stencil selection process is terminated at that step. This modification has the effect of limiting the order of the interpolation to the maximum possible value without interpolating across a discontinuity. In the example considered above, this restricts the order of accuracy to $m(N) = p-1$ between the two discontinuities. Upon grid refinement, spectral accuracy can be still be attained between the discontinuities since $p$ increases with $N$.

The modified stencil selection algorithm is summarized in Appendix 1. Note that the central stencil or stencils have been weighted as suggested by Shu [4]. There are probably other ways to limit the order of accuracy locally so as not to difference across discontinuities. One disadvantage of the above modification is that while interpolating an interval containing a discontinuity (such as $[x_k, x_{k+1}]$ in the above example) the order of the interpolation is frequently reduced to one. In all of the tests presented below this abrupt reduction in order did not create any problems such as oscillations or instabilities, although it does seem restrictive.

The choice of $m(N)$ and the threshold $1/\Delta x$ are somewhat arbitrary. The choice of the threshold plays the role of discontinuity detection in this scheme. A large threshold allows for better resolution in the smooth parts of the flow while risking an oscillatory interpolant near discontinuities. A small threshold allows for crisp resolution near discontinuities while risking a loss of accuracy in the smooth regions of the flow. The loss of accuracy in smooth regions is due to the fact that smooth oscillatory data may be "seen" as discontinuous by a small threshold. Some bounds on the size of the threshold may be based on the fact that for a smooth function the $k$th-divided difference is $O(1)/k!$ while for a jump discontinuity in the $p$th derivative ($0 \leqslant p \leqslant k$), the $k$th-divded difference is of order $(\Delta x)^{p-k}\,[w^{(p)}]$, where $[w^{(p)}]$ denotes the jump in the $p$th derivative. Hence, any quantity between $1/k!$ and $\Delta x^{p-k}$ can qualify as a threshold. Also, we may expect the threshold used for detection of ideal discontinuities, such as in interpolation, to be smaller than that used for detection of discontinuities that arise in gas dynamics. We have experimented with a few thresholds such as $1/\Delta x$, $1/(\Delta x)^2$, $2^k/(\Delta x)^2$, $k!/(\Delta x)^2$, $1/(\Delta x)^k$, etc. and found that $1/\Delta x$ gave the best performance for interpolation and $k!/(\Delta x)^2$ performed best for flow problems. More experimentation on a wide range of problems is necessary to determine the optimum threshold.

For spectral accuracy, $m(N)$ is required to be an increasing function of $N$. However, it is well known that the interpolant of a smooth function with $m(N) = 2N$ generally diverges for large $N$ (Runge phenomenon). Thus $m(N)$ cannot be too close to $2N$. Moreover, large values of $m(N)$ lead to large roundoff errors in the calculation of the divided differences which ultimately swamp any gains in accuracy from high orders. We have experimented with various functions and found that $m(N) = (N-1)/2$ yields reasonable results for the interpolation problem. When ENOV is used, along with a low order time integration scheme (as in ENOVRK below) we often encounter time step limitations that are prohibitively expensive. To alleviate this problem somewhat we have used $m(N) = \mathrm{Min}((N-1)/2, M_{\max})$, where $M_{\max}$ varies between 10 and 15.

## LINEAR ADVECTION

The ENOV interpolation scheme involves stencils that are very large and it is interesting to determine whether such large stencils lead to instability. To this end, we use the ENOV interpolation scheme to solve the linear advection problem given by

$$\begin{aligned} &u_t + u_x = 0 \\ &u(0, t) = u(2\pi, t), \qquad x \in [0, 2\pi] \\ &u(x, 0) = f(x). \end{aligned} \tag{7}$$

We prefer to work with the cell-averaged version of the difference equations. Let $\bar{u}_i(t)$ be the cell average of $u(x)$ defined by

$$\bar{u}_i(t) = \frac{1}{\Delta x} \int_{x_i - \Delta x/2}^{x_i + \Delta x/2} u(\xi, t)\, d\xi. \tag{8}$$

Integrating the pde over the cell results in the well-known semidiscrete form,

$$\frac{d\bar{u}_i}{dt} + \frac{1}{\Delta x}\left(u(x_{i+1/2}, t) - u(x_{i-1/2}, t)\right) = 0, \tag{9}$$

which can be integrated by a Runge–Kutta scheme. The fluxes $u(x_{i+1/2}, t)$ are approximated by $v(x^-_{i+1/2}, t)$, where $v(x)$ is the local approximate reconstruction of $u(x)$ from cell averages. This reconstruction is generally discontinuous at the cell faces, and the notation $v(x^-_{i+1/2}, t)$ stands for $v(x)$ evaluated at the left side of the face $x = x_{i+1/2}$. The reconstruction procedure is described in detail below. This scheme will be spectrally accurate in space and polynomial-order accurate in time. Spectral accuracy of the numerical solution can be demonstrated only by choosing the time step small enough so that the time differencing errors are subdominant compared to the spatial discretization errors. The advantage of this method is that the extension to systems is straightforward. In numerical tests described below, we have used a third-order Runge–Kutta scheme (Shu [5]) for time integration and refer to this as ENOVRK.

In the second approach, a scheme that is spectral in both space and time can be derived as follows: Integrating Eq. (9) over a time step we obtain the fully discrete form as

$$\bar{u}_i^{n+1} = \bar{u}_i - \lambda(f_{i+1/2} - f_{i-1/2}), \tag{10}$$

where $f$ is the exact flux defined by

$$f_{i+1/2} = \frac{1}{\Delta t}\int_0^{\Delta t} u(x_{i+1/2}, \xi)\, d\xi. \tag{11}$$

Again, the exact flux is approximated by the numerical flux $\hat{f}$ defined by

$$\hat{f}_{i+1/2} = \frac{1}{\Delta t}\int_0^{\Delta t} v(x^-_{i+1/2}, \xi)\, d\xi, \tag{12}$$

where $v(x)$ is the local approximate reconstruction of $u(x)$. The numerical flux is evaluated by the Cauchy–Kowalewsky method proposed in Harten [6]. The integrand of Eq. (12) is written as a taylor series in time and the time derivatives are replaced by the spatial derivatives by repeated differentiation of the pde. Term by term integration leads to

$$\hat{f}_{i+1/2} = \sum_{k=0}^{m-1} \frac{(-1)^k v^{(k)}_{i+1/2}\, \Delta t^k}{(k+1)!}, \tag{13}$$

where $v^{(k)}_{i+1/2}$ denotes the $k$th-spatial derivative of $v(x)$ at $x = x^-_{i+1/2}$.

The procedure of obtaining $v^{(k)}_{i+1/2}$ for $0 \leqslant k \leqslant m(N) - 1$ from the known cell averages is best accomplished using the primitive function method [6]. For ENOVRK, only $v^0_{i+1/2}$ is required. The primitive function $H(x)$ of $u(x)$ is given by

$$H(x) = \int_{-\Delta x/2}^{x} (u(\xi) - c)\, d\xi, \tag{14}$$

where $c$ is a constant chosen so that $H(x)$ is periodic whenever $u(x)$ is periodic, i.e.,

$$c = \int_{-\Delta x/2}^{2\pi - \Delta x/2} u(\xi)\, d\xi = \frac{\Delta x}{2\pi} \sum_{i=-N}^{N} \bar{u}_i; \tag{15}$$

$H(x)$ is known at the half nodes as

$$H(x_{j+1/2}) = \Delta x \sum_{k=-N}^{j} \bar{u}_k - c(j + 1 + N)\, \Delta x. \tag{16}$$

The ENOV scheme can now be used to interpolate $H(x_{j+1/2})$. For $x \in [x_{j-1/2}, x_{j+1/2}]$, let $m(N)$ and $x_{i+1/2}$ be the order of accuracy and leftmost point of the stencil as determined by the ENOV interpolation procedure described earlier. In the local variable

$$\eta = (x - x_{i+1/2})/\Delta x, \tag{17}$$

the ENO interpolant can be written as

$$H(\eta) = d_0 + \sum_{l=1}^{m} \prod_{k=0}^{l-1} (\eta - k)\, d_l, \tag{18}$$

where $d_k$ are the normalized divided differences of $H$. As in Harten [6, Appendix 1] with a view to repeated differentiation, Eq. (18) can be written as

$$H(\eta) = \sum_{k=0}^{m} a_k \eta^k, \tag{19}$$

where

$$a_k = \sum_{q=k}^{m} S^k_q d_q \tag{20}$$

and $S^k_q$ is the Stirling number [7] of the first kind. Repeated differentiation of Eq. (19) and rescaling gives

$$\frac{d^k H}{dx^k} = \sum_{l=k}^{m} \frac{a_l l!\, (x - x_{i+1/2})^{l-k}}{(l-k)!\, \Delta x^l}, \qquad k = 0, m. \tag{21}$$

Finally, the derivatives of $v$ can be computed as

$$v^{(k)}_{j+1/2} = \left.\frac{d^{k+1} H}{dx^{k+1}}\right|_{x = x_{j+1/2}} + c\delta^0_k, \qquad k = 0, m-1, \tag{22}$$

from which the numerical flux (Eq. (13)) can be calculated.

The scheme described above (ENOVCK) has spatial and temporal accuracy of $m(N)$ which increases with $N$. Hence, the scheme gives spectral-like accuracy in space and time. However, due to algebraic complexity, it is not easy to extend this to even scalar nonlinear equations. Furthermore, the calculation of the coefficients $a_k$ becomes

increasingly ill-posed for large $m$ and is subject to large roundoff errors as it is equivalent to inversion of the $m \times m$ Vandermonde matrix.

## EULER EQUATIONS

The extension of the ENOVRK scheme to the 1D Euler equations is quite straightforward and amounts to little more than incorporating a variable order $m(N)$ and the modified stencil selection procedure described earlier into a standard ENO scheme. The reader is referred to Refs. [3, 6] for details. Here we will briefly point out some differences from convection.

As is standard practice, we use local characteristic variables [3] to interpolate. The constant $c$ in the primitive function $H(x)$ is zero here, since $u(x)$ is not periodic. For gas dynamics, both the values of $v(x)$ at $x = x^-_{i+1/2}$ and $x = x^+_{i+1/2}$ are required. These values are the left and right states for a Riemann problem whose solution at $x = x_{i+1/2}$ gives the numerical flux. The exact Riemann solver by Gottlieb [8] was used in this study.

## NUMERICAL TESTS

We describe below various numerical tests on both the USE scheme and the ENOV scheme.

### 1. *Interpolation of a Smooth Function*

We consider interpolating the smooth function $u(x) = \sin^4(x)$ on $x \in [0, 2\pi]$ with the USE and ENOV schemes. For the former, no discontinuities are detected and a 10th-order filter is used. For the latter, we use a threshold of $1/\Delta x$, $m = (N-1)/2$, and enforce periodic conditions at $x = 0, 2\pi$. For purposes of comparison we also present results with a fixed third-order ENO scheme (ENO3), which corresponds to piecewise cubic interpolation. The point errors are defined as in Eq. (1) and the global maximum error is shown as a function of $N$ in Table I. As expected, for the USE scheme the maximum error is essentially machine zero once the modes in the initial condition are resolved. The ENOV scheme clearly shows spectral accuracy beyond $N = 8$ and the order exponent of the ENO3 scheme asymptotes to 4 as expected. For this case, the USE scheme is much superior, since the USE scheme achieves machine zero with $N = 4$ while the ENOV scheme requires $N = 36$ to reduce the maximum error to machine zero.

**TABLE I**

Interpolation of $\sin^4(x)$ by Various Schemes

| $N$ | Max. error | Order |
|---|---|---|
| | USE scheme | |
| 2 | 0.250 | — |
| 3 | 0.250 | 0 |
| 4 | 1.38(−17) | 139.77 |
| | ENOV scheme | |
| 4 | 0.189 | — |
| 8 | 1.838(−2) | 3.66 |
| 16 | 1.711(−5) | 10.52 |
| 32 | 6.928(−13) | 25.11 |
| | ENO3 scheme | |
| 4 | 0.107 | — |
| 8 | 0.838(−2) | 2.76 |
| 16 | 1.957(−3) | 3.37 |
| 32 | 1.347(−4) | 3.95 |
| 64 | 8.766(−6) | 3.99 |

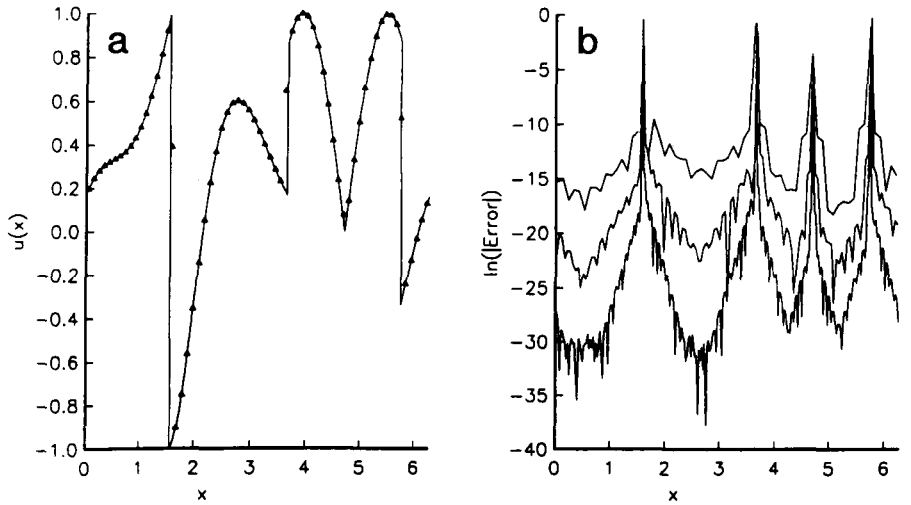


**FIG. 1.** (a) USE interpolation with $N = 32$. (b) Log of point errors with $N = 32, 64, 128$, $m = 3, 21 = 10$.

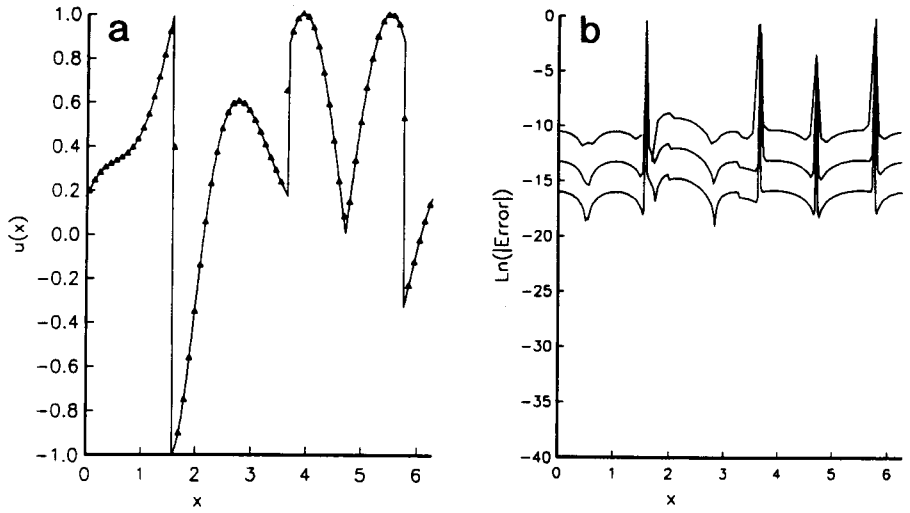


FIG. 2. (a) ENO3 interpolation with $N=32$. (b) Log of point errors with $N=32, 64, 128$, $m=3$.

2. *Interpolation of a Discontinuous Function*

The chosen function is essentially the same as the one in Harten [9] mapped into $[0, 2\pi]$. Let $z=x/\pi-3/2$. Then the function is given by

$$\begin{aligned} u(z) &= -z\sin(3\pi z^2/2), && -1<z<-\tfrac{1}{3} \\ &= |\sin(2\pi z)|, && -\tfrac{1}{3}<z<\tfrac{1}{3} \\ &= 2z-1-\sin(3\pi z)/6, && \tfrac{1}{3}<z<1. \end{aligned} \tag{23}$$

For $z<-1$, $u(z)=u(z+2)$. The function has three function discontinuities and several derivative discontinuities. Figure 1 shows the results of interpolation using the USE scheme. A sharp nonoscillatory interpolation is obtained as shown in Fig. 1a. In a plot of the logarithm of the point errors, spectral accuracy can be ascertained by the unequal spacing between curves as the number of points is doubled. Comparing the plot of the log error (Fig. 1b) obtained, with the USE scheme, with that obtained from ENO3 (Fig. 2b), we seem to observe evidence of spectral accuracy in the smooth regions between the discontinuities. For the ENOV scheme a threshold of $1/\Delta x$ and $m(N)=(N-1)/2$ was used. The results from the ENOV scheme are shown in Fig. 3 and seem to be superior to the USE scheme. To reach close to machine zero in the smooth regions the USE scheme required $N=128$, whereas the ENOV scheme required only $N=32$.

As a further test, an ENO scheme of order $m(N)$ but *without* any modifications to the stencil selection procedure was also tested. The results are shown in Figs. 4a, b. The loss of spectral accuracy in certain regions between discontinuities is clearly visible in Fig. 4b.

To compare efficiencies, a real FFT routine (from the IMSL math library) was used to compute the Fourier coefficients and the function values (instead of Eqs. (4, 5)) for

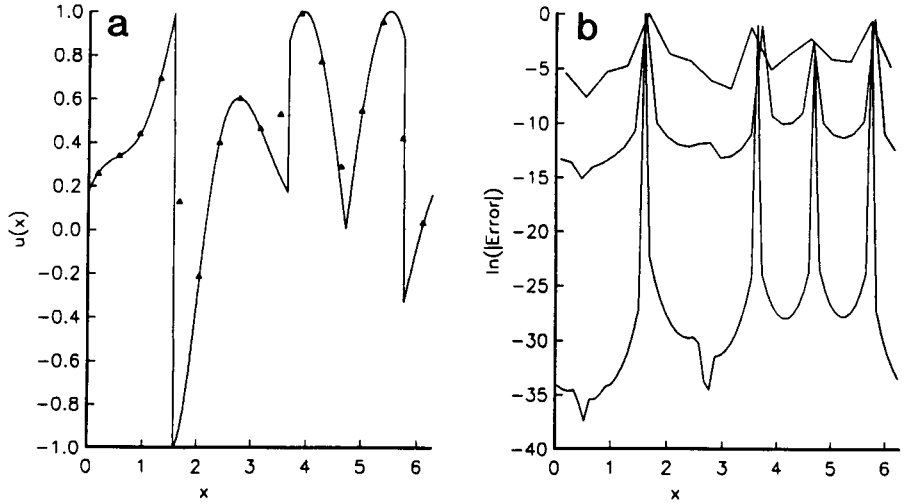


FIG. 3. (a) ENOV interpolation with $N=8$. (b) Log of point errors with $N=8, 16, 32$, $m$ variable.

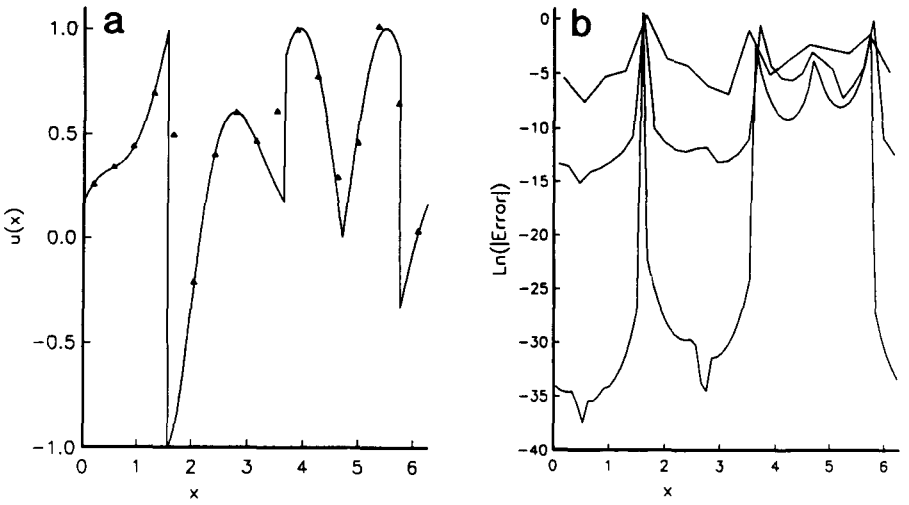


**FIG. 4.** (a) ENOV interpolation without stencil selection modification, $N = 8$. (b) Log of point errors with $N = 8$, 16, 32, $m$ variable.

the USE scheme. For the ENOV scheme a threshold of $1/\Delta x$ and $m(N) = (N-1)/2$ (with no upper limit) was used. All computations were carried out in single precision on the Cray-YMP without any special effort at vectorization. In particular, the field loop over all cells (i.e., the loop over $j$ in Appendix 1) did not vectorize in these computations. Table II shows the CPU times for the various schemes. The ENOV scheme is between 2.5 to 2 times faster than the USE scheme for the grids tested. However, the gap narrows for larger $N$. With the third-order ENO scheme, the error in the smooth region on the finest grid ($N = 162$) is on the order of $10^{-8}$ and takes roughly 0.056 s. In comparison, with the ENOV scheme, with $N = 37$, the error in the smooth regions is on the order of $10^{-15}$ and takes only 0.017 s. Thus, for this very simple problem, the higher order accuracy is well worth the extra effort.

### 3. *Advection of a Discontinuous Function*

The ENOVRK and ENOVCK were used to solve the problem of linear advection over a period of the function given in Eq. (23). To demonstrate spectral accuracy with ENOVRK the time step needs to be chosen small enough so that time differencing errors are negligible when compared to the spatial differencing errors. Thus, the time step in these simulations was reduced sequentially in such a way that further reduction of the time step did not significantly reduce the error in the smooth regions. This results in a small time step equal to $\Delta t = 2\pi/1800$. Once this time step was determined, the discontinuous initial function given by Eq. (23) was advected for one period for $N = 8$, 16, 32, and 64 with the same time step. As mentioned earlier, a larger threshold of $k!/\Delta x^2$ and $m(N) = (N-1)/2$ was used. The results are shown in Figs. 5a, b. We seem to observe spectral accuracy in the smooth regions, although this is not as clear as for interpolation.

**TABLE II**

Comparison of the Efficiencies of Various Schemes

| $N$ | USE | ENOV | ENO3 |
|---|---|---|---|
| 37 | 0.048 | 0.017 | 0.015 |
| 62 | 0.083 | 0.030 | 0.023 |
| 112 | 0.152 | 0.061 | 0.040 |
| 162 | 0.222 | 0.112 | 0.056 |

*Note.* CPU times are in Cray-YMP seconds.

It is worth mentioning that such small time steps are *not* due to stability constraints. Numerical experiments indicate that the ENOVRK scheme is stable for $\Delta t/\Delta x \leqslant 0.5$ with $M_{\max} = 15$. However, at such large time steps the errors due to time differencing completely overshadow the spatial differencing errors so that spectral accuracy cannot be observed.

The results from ENOVCK are shown in Figs. 6a, b. Grids with $N = 8$, 16, and 32 were used in the study with the same threshold and $m(N)$ as above. Spectral convergence is discernable in the smooth regions of the function. However, grid refinement beyond $N = 32$ gave rise to generally poorer results. We speculate that this is due to roundoff errors caused by the evaluation of factorials and Stirling numbers with magnitudes on the order of machine infinity. It may be possible to combine Eqs. (13), (18), and (19) into a form that is less susceptible to roundoff errors. This will be investigated in future work. A recent related paper by Tal-Ezer [10] addresses precisely the nonconvergence of high order polynomial interpolation in Newton form.

The increased resolution of high order schemes is further illustrated in Fig. 7, where a solution with ENOVRK on a coarse grid (Fig. 7a) is compared with a solution with third-order ENO (Fig. 7b) under identical conditions. The

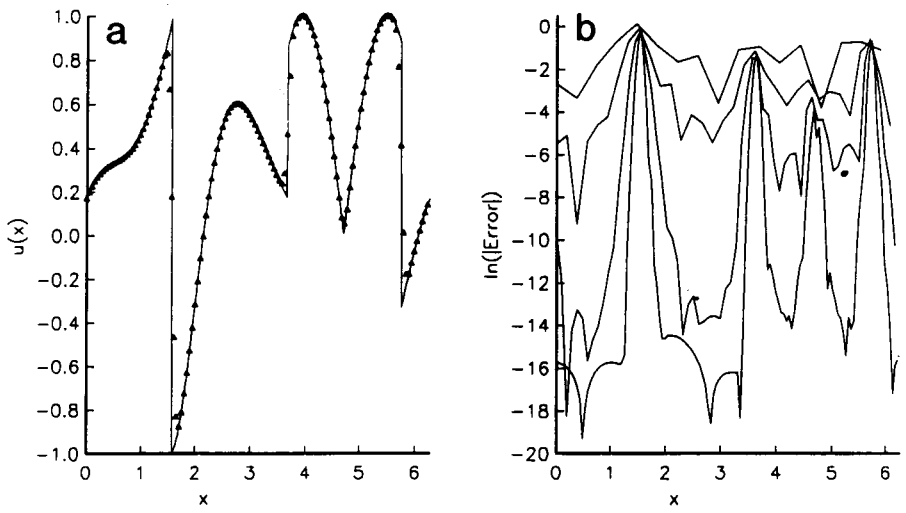


FIG. 5. (a) Advection over one period with ENOVRK; $Dt = 2\pi/1800$, $N = 64$. (b) Log of point errors; $N = 8, 16, 32, 64$, $m$ variable.

increased resolution is clearly visible, especially between discontinuities.

4. *Inviscid Burgers' Equation*

We solve the initial value problem given by

$$u_t + \frac{(u^2)_x}{2} = 0 \tag{24}$$

in the interval $x \in [0, 6]$ with initial conditions given by

$$u(x, 0) = 0.3 + 0.7 \sin \frac{\pi x}{3} \tag{25}$$

and periodic boundary conditions using an obvious extension of ENOVRK. The cell faces here are given by $x_i = 6(i-1)/N$, $i = 1, N+1$. An iterative exact solution to this problem is readily obtained, as is the exact Riemann solver. We solve this problem with $m = \text{Min}((N-1)/2, 15)$ and a threshold of $k!/\Delta x^2$. Again, the time step is chosen small enough so that the time differencing errors become subdominant. A sharp nonoscillatory solution is obtained with as few as eight points (Fig. 8a). The plot of the log errors (to the base 10) is shown in Fig. 8b for $N = 8, 16, 32$. Again, we seem to observe spectral accuracy in the smooth regions.

These results can be compared with the results of Cai and Shu [3] (who solve it on the domain $[0, 2\pi]$) and Sidilkover and Karniadakis [11], who use a nonoscillatory spectral element method. With the scheme of Cai and Shu, an error level of $10^{-10}$ is achieved with approximately 250 points (Fig. 4a of Ref. [3]), while Sidilkover and Karniadakis achieve this error level with approximately 160

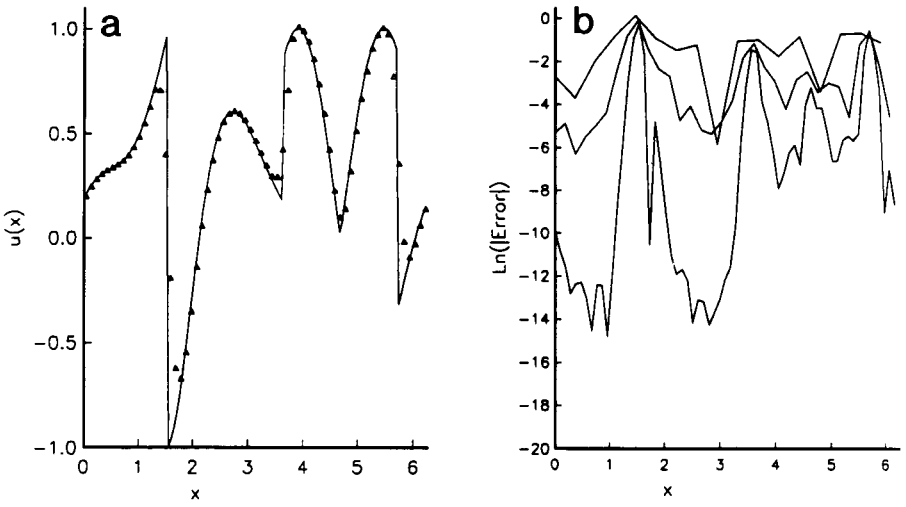


FIG. 6. (a) Advection over one period with ENOVCK; CFL = 0.2, $N = 32$, $m$ variable. (b) Log of point errors with $N = 8, 16, 32$, $m$ variable.

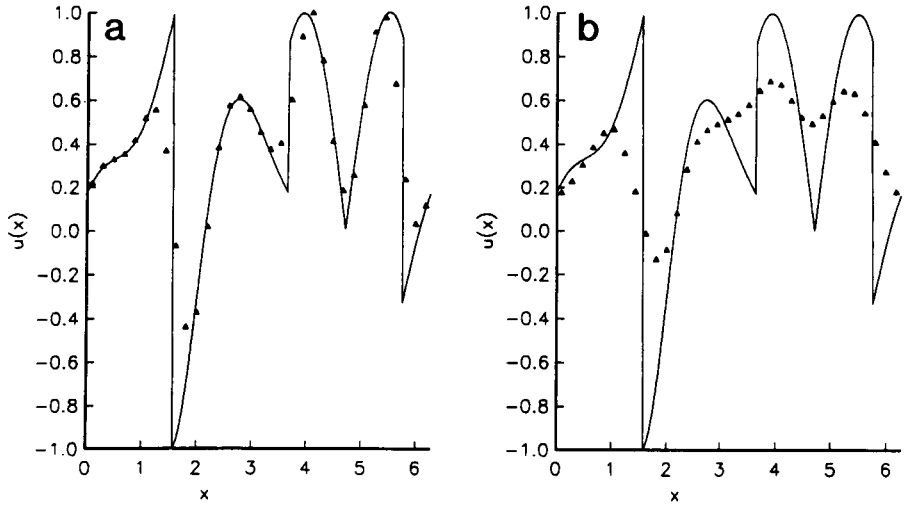


**FIG. 7.** (a) Advection over one period with ENOVRK; $Dt = 2\pi/1800$, $N = 16$, $m$ variable. (b) Same as (a) except $m = 3$.

points (Fig. 9 of Ref. [11]). In contrast, the same error level is achieved by the ENOV scheme with 32 points (Fig. 8b).

### 5. *Interaction of a Moving Shock with a Density Disturbance*

This is the same problem as in Cai, Gottlieb, and Harten [12] which was first introduced in Shu and Osher [13] with slightly different parameters. This test problem contains both smooth structure and discontinuities and is thus a good test problem for higher order methods. The domain of the problem is $-1 \leqslant x \leqslant 1$, and a uniform grid of 200 points was used in all cases. Due to severe time step restrictions, we chose $m(N) = \text{Min}((N-1)/2, 10)$ for these computations. The initial conditions are

$$\begin{aligned}(\rho_L, u_L, p_L) &= (3.857143, 2.629369, 10.3333) \\ &\text{for} \quad x < -0.8 \\ (\rho_R, u_R, p_R) &= (1 + \varepsilon \sin(5\pi x), 0, 1) \\ &\text{for} \quad x > -0.8,\end{aligned} \tag{26}$$

where $\rho$, $u$, $p$ are the density, velocity, and pressure, respectively. The ratio of specific heats $\gamma = 1.4$ and $\varepsilon = 0.2$. When $\varepsilon = 0$, this is a pure Mach 3 shock moving to the right. As there is no known exact solution to this problem, a solution with a third-order ENO scheme with 800 points is used instead.

The results, presented in Figs. 9a, b, show the density field at $t = 0.36$. The solid line is the ENO3 solution with 800

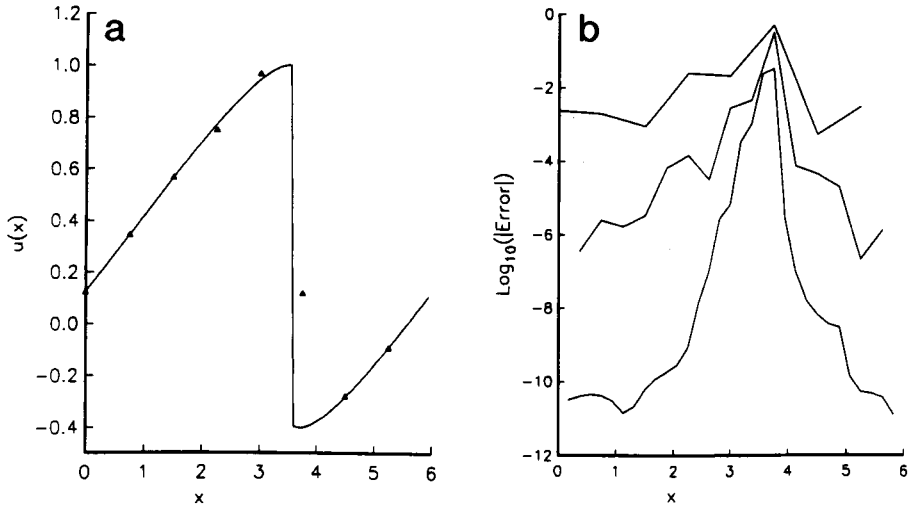


**FIG. 8.** (a) ENOV solution to Burgers equation with eight points; $Dt = 2/1000$. Threshold $= k!/dx/dx$, $t = 2$. (b) Log of point errors with $N = 8, 16, 32$.

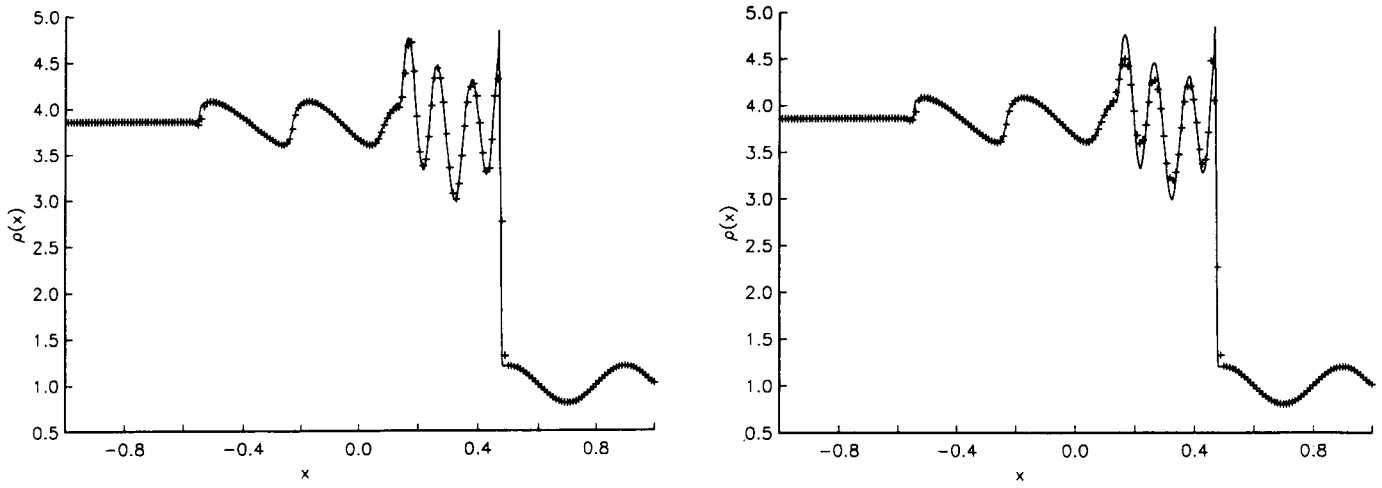


**FIG. 9.** (a) Density profile at $t = 0.36$. $N = 200$, threshold $= k!/dx/dx$, $Dt = 0.36/400$, $Rk3$. (b) Same as (a) except threshold $= 1/dx$.

points. With the threshold of $1/\Delta x$ (Fig. 9b), it can be seen that the postshock density oscillations are clearly underresolved while with the threshold of $k!/\Delta x^2$ (Fig. 9a), we obtain full resolution of these oscillations. In Ref. [12] a cell averaging Chebyshev spectral method (CAC) obtains full resolution of the solution with 220 points. For this problem, it thus appears that the results of the ENOV scheme (with the second threshold) are comparable in resolution to results obtained using the CAC spectral method.

## CONCLUSIONS

Numerical experiments confirm that both the USE scheme and the ENOV scheme give interpolations that are nonoscillatory and achieve spectral accuracy in smooth regions. The new scheme proposed herein (ENOV) provides an easy and efficient way to achieve spectral accuracy in smooth regions without explicit discontinuity detection and conventional smoothing. When applied to convection and 1D gas dynamics, the new scheme gives results comparable in accuracy and efficiency to earlier results using spectral schemes.

Both schemes involve arbitrary parameters related to discontinuity detection, which remains a problem. Further analysis and testing is required in this area before spectral nonoscillatory schemes achieve the reliability of traditional nonoscillatory upwind schemes.

## APPENDIX 1

Let $d(k, i)$ be the $k$th-order divided difference with leftmost point $x_i$, i.e.,

$$d(k, i) = u[x_i, ..., x_{i+k}]$$

and let $is(k)$ for $k = 1, ..., m$ denote the leftmost point of the stencil at each stage of the stencil selection process and let $ic(j)$ denote the leftmost point in the linearly stable centered stencil. The conventional stencil selection algorithm to find $is(m)$ is

```
is(1) = j
do 100 k = 1, m − 1
    if(is(k) > ic(j)) then
        if(2 |d(k + 1, is(k))| > |d(k + 1, is(k) − 1)|) then
        is(k + 1) = is(k) − 1
        else
        is(k + 1) = is(k)
        endif
    else
        if(|d(k + 1, is(k)| > 2 |d(k + 1, is(k) − 1)|) then
        is(k + 1) = is(k) − 1
        else
        is(k + 1) = is(k)
        endif
    endif
100     continue
```

We propose modifying this algorithm to include a locally varying order $m = m(N)$ and a check on the absolute magnitude of the divided differences. The modified algorithm may be written as

```
m = m(N)
is(1) = j
do 100 k = 1, m − 1
d_min = min(|d(k + 1, is(k) − 1)|, |d(k + 1, is(k))|)
  if(d_min ≥ 1/Δx) then
  m = k
  go to 101
```

```
      else
          if(is(k)   >   ic(j)) then
              if(2 |d(k+1, is(k)| > |d(k+1, is(k)-1|) then
              is(k+1) = is(k)-1
              else
              is(k+1) = is(k)
              endif
          else
              if(|d(k+1, is(k)| > 2 |d(k+1, is(k)-1)|) then
              is(k+1) = is(k)-1
              else
              is(k+1) = is(k)
              endif
          endif
      endif
  100 continue
  101 continue
```

## ACKNOWLEDGMENTS

The author thanks his colleagues at NASA Lewis for several interesting discussions. This work was supported by NASA Lewis Research Center under Contract NAS3-25266 with Dr. D. R. Reddy as monitor.

## REFERENCES

1. D. Gottlieb, L. Lustman, and S. A. Orszag, *SIAM J. Sci. Stat. Comput.* **2**, 296 (1981).
2. W. Cai, D. Gottlieb, and C.-W. Shu, *Math. Comput.* **52**, 186, 389 (1989).
3. W. Cai and C.-W. Shu, *J. Comput. Phys.* **104**, 427 (1993).
4. C.-W. Shu, *J. Sci. Comput.* **5**, No. 2 (1990).
5. C.-W. Shu and S. Osher, *J. Comput. Phys.* **77**, 439 (1988).
6. A. Harten, B. Engquist, S. Osher, and S. R. Chakravarthy, *J. Comput. Phys.* **71**, 231 (1987).
7. M. Abramowitz and I. A. Stegun, *Handbook of Mathematical Functions* (Dover, New York, 1970), p. 824.
8. J. J. Gottlieb and C. P. T. Groth, *J. Comput. Phys.* **78**, 437 (1988).
9. A. Harten, *J. Comput. Phys.* **83**, 148 (1989).
10. H. Tal-Ezer, *SIAM J. Sci. Stat. Comput.* **12**, No. 3, 648 (1991).
11. D. Sidilkover and G. E. Karniadakis, *J. Comput. Phys.* **107**, 10 (1993).
12. W. Cai, D. Gottlieb, and A. Harten, ICASE Report No. 90-27 (Institute for Computer Applications in Science and Engineering, NASA Langley Research Center, Hampton, 1990).
13. C.-W. Shu and S. Osher, *J. Comput. Phys.* **83**, 32 (1989).